AIP Journal of Applied Physics

Monte Carlo simulations of sputter atom transport in lowpressure sputtering: The effects of interaction potential, sputter distribution, and system geometry

A. M. Myers, J. R. Doyle, and D. N. Ruzic

Citation: J. Appl. Phys. **72**, 3064 (1992); doi: 10.1063/1.351464
View online: http://dx.doi.org/10.1063/1.351464
View Table of Contents: http://jap.aip.org/resource/1/JAPIAU/v72/i7
Published by the American Institute of Physics.

Monte Carlo simulations of sputter atom transport in low-pressure sputtering: The effects of interaction potential, sputter distribution, and system geometry

A. M. Myers[a] and J. R. Doyle[b]
The Coordinated Science Laboratory, University of Illinois, Urbana, Illinois 61801

D. N. Ruzic
Department of Nuclear Engineering, University of Illinois, Urbana, Illinois 61801

(Received 12 March 1992; accepted for publication 16 June 1992)

A comparative study of the various model assumptions in Monte Carlo simulations of low-pressure sputter-atom transport is presented. The few-collision conditions and actual "racetrack" magnetron geometry, typical of low-pressure magnetron sputtering, are emphasized. For the gas phase scattering problem, a comparison is made between hard sphere, Lennard–Jones 6-12, and Abrahamson Thomas–Fermi–Dirac [Phys. Rev. **178**, 76 (1969)] interatomic potentials. The hard sphere potential results in both a significantly lower energy distribution and a more diffuse angular distribution for the depositing flux, as compared with the more realistic "softer" potentials. Because energy-dependent cross sections are obtained when using the 6-12 and Abrahamson potentials, an "energy filtering" effect is observed, i.e., high-energy particles arrive at the substrate preferentially to those at low energy. It is concluded that the hard sphere model will lead to serious errors in both the energy and angular distributions of the arrival flux, and that the 6-12 and Abrahamson potentials yield results that are similar to each other. For the nascent sputter distribution, fractal TRIM (transport of ions in matter) simulations are compared to the analytic Thompson distribution. While both distributions give nearly identical results for the angle-integrated fluxes, the fractal TRIM distribution shows a strong angular dependence of the energy distribution. The implications of this effect for finite geometry systems are discussed.

I. INTRODUCTION

Sputtering is a firmly established technique for the deposition of a wide variety of thin films. It is well known that the energy and angular distributions of the arrival flux can have profound effects on the film microstructure and other properties. In turn, process parameters such as working gas pressure and system geometry will have significant effects on these distributions, particularly in the lower pressure regimes when the sputtered gas is not completely thermalized at the background gas temperature. Consequently, there has been considerable effort over the past two decades to model the effects of process parameters on the deposition flux in sputter deposition. Studies[1–9] have used various combinations of interatomic interaction models, nascent sputter distributions, and system geometries, usually combined with Monte-Carlo procedures, in order to model the gas phase transport. To date, however, there has been no systematic study of the effects of the various model assumptions used in these simulations. Such a comparative study is the aim of the present work.

A review of the seminal contributions to date has recently been presented by Turner *et al.*[1] The papers most relevant to the present work are briefly summarized here. Motohiro[2,3] used hard sphere potentials, as well as the more accurate potentials calculated by Abrahamson,[10] in order to describe gas phase scattering, and a Thompson distribution[11] to describe particle ejection from the target. By analyzing the spatial distribution of film growth he concluded that his results were independent of the potential used to describe scattering and that the best agreement with the deposition profiles is obtained with a $\sin^2\theta$ angular ejection profile for the nascent sputter distribution. Vidal and Asomoza[4] used a hard sphere potential, infinite parallel plates, and the Thompson distribution. Turner *et al.*[1] used an infinite parallel-plate geometry, a Lennard–Jones 6-12 potential, and the Thompson distribution. They determined the spatial densities and average kinetic energies of the sputtered particles, as functions of pressure and the distance from the cathode. The researchers were able to obtain results in good agreement with experimentally determined longitudinal velocity distributions of the sputtered atoms measured by Doppler broadening in a parallel-plate reactor. We have recently obtained results[5,6] for the angular and energy distributions of the arrival flux at a substrate, by using a realistic chamber geometry, fractal TRIM simulations[12] for the sputter distribution, and the so-called "Universal" potential[13] (originally developed to calculate ion stopping powers in solids) to describe the gas phase scattering problem.

Despite the relatively high level of activity in this field, with the exception of Motohiro's comparison of deposition profiles,[3] there has been no systematic study of the effects of the various model assumptions on the energy and angular distributions of the deposition flux. If the distributions

[a]Present address: Intel Corporation, Hillsboro, OR 979124-6497.
[b]Present address: Physics Department, Macalester College, St. Paul, MN 55105-1899.

 0021-8979/92/193064-08$04.00

are insensitive to the choice of these assumptions, this would allow modelers to use, for example, hard sphere and Thompson analytical formulations, which are not only much easier than the others to implement, but would also greatly decrease the overall computation time. On the other hand, if variances between the results of different potentials are found, then previous results must be critically reviewed in order to determine their applicability.

In general, three regimes for the gas phase transport can be considered, characterized by the product pd, where p is the working gas pressure and d is the target-to-substrate distance.[14] In the high-pressure regime, where $pd \gg 50$ mTorr cm, the large number of collisions with background gas that occur while the sputtered particle is in transit between the target and substrate will thermalize the sputtered atoms. The film growth flux thus arrives with a nearly iostropic angular distribution and an energy distribution which is close to that of the background gas, and is not sensitive to the nascent sputter distribution leaving the target. Furthermore, the results are relatively insensitive to the form of the interatomic scattering potential, since the numerous collisions "wash out" the details of the interaction. This regime is characteristic of high-pressure diode sputtering, for example. In the very-low-pressure regime, where $pd \ll 5$ mTorr cm, the number of collisions that occur with the background gas are negligible. As a result the deposition flux distributions are closely related to the nascent sputtered distributions. The geometry of the system may also have a large effect on the arrival flux distributions. Such a situation occurs in ion beam sputtering. In the intermediate regime, where $5 < pd < 50$ mTorr cm, there are a small number of collisions, so that the distributions can be changed significantly from the nascent distributions. However, a significant portion of the flux retains memory of its original distribution, and the resulting deposition flux distributions are expected to be sensitive both to the nascent sputter distributions and the gas phase scattering potentials. In modeling this intermediate regime, which is commonly used in magnetron sputtering, it is therefore important to determine the influence of sputter distributions, gas phase scattering potentials, and system geometry on the substrate arrival flux distributions.

In this work a detailed comparison is made of the various types of interatomic potentials used in the literature for gas phase collisions in the intermediate pd regime. In addition, the difference between the analytic Thompson distribution and a more accurate fractal TRIM simulation for the nascent sputter distribution are studied. These results are relevant for both the low and intermediate pd regimes. Finally, the effects of a finite system geometry, in contrast to the infinite parallel plates typically used, are considered. For definitiveness, and because of its relevance to our mass spectrometry studies,[15] the case of silicon sputtered by argon in a realistic circular magnetron geometry will be considered. For all of the aforementioned comparisons, the discussion will focus on the higher energy (>0.25 eV) part of the substrate arrival flux distribution, since this is the portion most sensitive to the model parameters. Although the present model could easily be extended to encompass the lower energy part of the distribution, this would greatly increase computation time. In addition, this regime is very sensitive to the low-energy (attractive) part of the interatomic potential. An accurate treatment of this part of the potential requires sophisticated quantum mechanical methods, and has not been carried out for the argon-silicon case of interest here. Instead, the lower-energy part of the distribution has been accounted for by using approximations described below.

II. PROCEDURE

A. Gas phase scattering

In order to accurately compare the results of different potentials, sputter distributions, and the effect of system geometry, it is necessary to evaluate the complete angular and energy distributions at the substrate. For the gas phase transport a classical description of the scattering dynamics using analytic potentials has been applied. Monte Carlo sampling procedures are used to treat an ensemble of particles. Although the potentials used in this study do not exhaust all possibilities, they comprise three representative cases that have been used in the sputtering literature thus far.

For a given spherically symmetric atom–atom interaction potential and specified initial conditions of relative kinetic energy and impact parameter, the scattering problem is completely determined. For the relative scattering angle in the center of mass frame,[16]

$$\theta_{\mathrm{com}} = \pi - 2b \int_{r_0}^{\infty} \frac{dr}{r^2\{1-[V(r)/E_{\mathrm{com}}]-(b^2/r^2)\}^{1/2}}, \tag{1}$$

where r_0 is determined from the implicit equation

$$b^2 = r_0^2 \left(1 - \frac{V(r_0)}{E_{\mathrm{com}}}\right). \tag{2}$$

In general both Eqs. (1) and (2) must be solved numerically. In practice a three-dimensional array of b, E (the energy of the silicon in the lab frame) and θ_{com}, resulting from the integration of Eq. (1), is generated and stored in a look-up table. Thus, for a given E, θ_{com} is calculated for b values ranging from $b=0$ to $b=b_{\max}$, where $b_{\max}$ is the smallest impact parameter that produces a deflection of less than 1°. The total scattering cross section at this energy is then defined by $\pi b_{\max}^2$.

To begin a trajectory, the sputtered atom is released from the target surface with its energy and angle determined by either the Thompson distribution or the fractal TRIM simulation. In the former case, the rejection method of sampling with the modification used by Turner *et al.*[1] was used. The TRIM simulation data explicitly give the distribution in discrete form. These distributions will be discussed in greater detail in Sec. II C. The location of the first collision in the gas is determined by assuming a distribution $P(r)$ of free paths r,

$$P(r) = \exp[r/\lambda(E)], \tag{3}$$

where $\lambda(E)$ is the (energy-dependent) mean free path given by the relation $\lambda(E)=(N\pi b_{\max}^2)^{-1}$, and N is the argon density. To determine the free path r, a random number RN1 is generated and the free path is calculated from $r=\lambda(E)\ln(\mathrm{RN1})$, according to standard Monte Carlo procedure.[17] Once a collision has occurred, a second random number RN2 is generated and b is calculated from the relation $b=b_{\max}(\mathrm{RN2})^{1/2}$. Equation (1) then gives the polar scattering angle, and the energy transferred is given by[16]

$$E_f=\frac{E_{\mathrm{int}}M_t^2}{(M_g+M_t)^2}\left[\cos(\theta_{\mathrm{lab}})+\sqrt{(M_g/M_t)^2-\sin^2(\theta_{\mathrm{lab}})}\right], \tag{4}$$

where M_t is the mass of the background gas argon, M_g is the mass of the sputtered species silicon, and E_{int} is the energy of the silicon atom before the collision. A third random number RN3 is used to generate the azimuthal angle $\phi=2\pi(\mathrm{RN3})$. Transformation back to the laboratory frame completes the scattering event, and a new free path, corresponding to the new energy, is determined as above. The cycle continues until either the trajectory intercepts the substrate area, in which case the energy and intercept angle are recorded, or the trajectory intercepts the chamber boundaries and the silicon is considered lost. A new atom is then launched from the target and the simulation is repeated.

Since we assume that the argon atoms are initially stationary, the simulation is not valid if the energy of the sputtered silicon becomes comparable to kT of the background gas. Although extension of the present simulation to energies lower than kT is straightforward, a significant increase in computation time would be required. In addition, the low-energy transport is very sensitive to the more uncertain low-energy attractive part of the potential. On the other hand, the fraction of the sputtered flux that degrades to low energy is an important parameter that characterizes the gas interatomic potential, and it is therefore useful to estimate its contribution to the total arrival flux. In this simulation, if the energy of an atom falls below 0.25 eV within the chamber boundaries, its location is noted and the atom is considered "quasithermalized." The contribution of these quasithermals to the deposition flux can then be calculated using a diffusive transport model.[6,18] The initial quasithermal distribution is used as the source term, and Fick's law is integrated assuming a unity sticking coefficient at all surfaces. The results yielded by such a model probably underestimates somewhat the contribution of quasithermals to the total flux, since it is expected that the atoms would have directed velocity towards the substrate. Nevertheless, the quasithermal concept is a useful qualitative characterization of the gas phase interaction potential.

B. Scattering potentials

Figure 1 shows the scattering potentials used in this study. The hard sphere potential, with its radius typically derived from viscosity measurements,[19] has the advantage

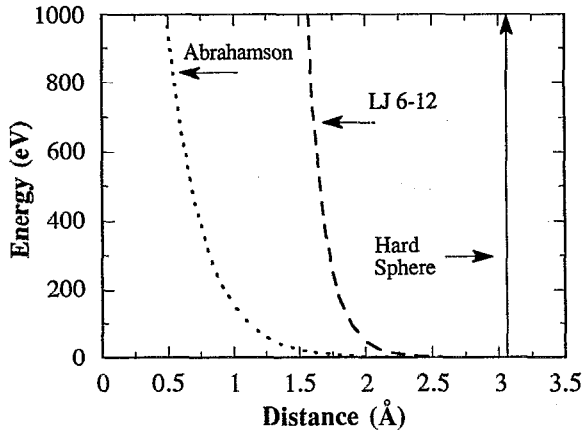

FIG. 1. Gas phase silicon-argon interaction potentials vs interatomic separation.

that Eqs. (1) and (2) can be solved analytically. This type of potential is a reasonable approximation for the low-energy many-collision limit. In the higher energy, few collision case studied here the hard sphere interaction is expected to be a poor approximation. A more realistic form for the potential is the Lennard–Jones 6-12 formulation,[19] given by

$$V(r)=2\varepsilon[(\sigma/r)^6-(\sigma/r)^{12}]. \tag{5}$$

In this case, the r^{-6} term corresponds to the long-range Van der Waals interaction between neutral molecules. Thus, this potential should treat the low-energy part of the interaction much more accurately than does the hard sphere, and is commonly used for accurate transport at thermal energies. The r^{12} term is included in order to account for repulsion at small interatomic separations, but does not otherwise have a rigorous justification. The parameters ε and σ for argon and silicon are taken to be 53 meV and 3.146 Å, respectively.[20] Although somewhat "softer" (i.e., less steep) than a hard sphere, this form of the repulsion is still much steeper than that found by more rigorous calculation, and hence may not give accurate results in the few-collision high-energy limit.

There have been several calculations to obtain more accurate potentials at energies in the few eV range and above. Abrahamson[10] has used the Thomas–Fermi–Dirac method to calculate the repulsive part of atom–atom potentials for 92 elements. He found that when $0.8<r<1.9$ Å the potentials could all be expressed in the Born–Mayer form

$$V(r)=A\exp(-br). \tag{6}$$

For the silicon-argon case $A=5942$ eV and $b=3.664$ Å^{-1}.[10] In Fig. 1, the much "softer" nature of this potential, as compared to the hard sphere and 6-12 potential, is evident. This feature has the consequence that the effective total cross section is strongly energy dependent. At low energies the Abrahamson potential can, in principle, be modified to account for the long-range Van der Waals interaction by using the expression

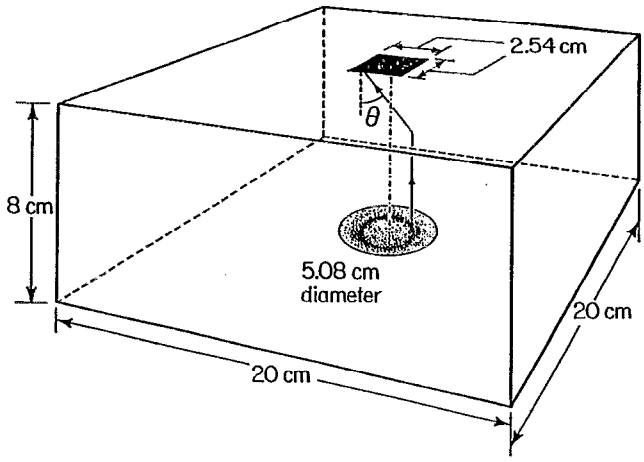

FIG. 2. Geometry used in the simulations. A 5.08-cm-diam sputtering target with a 2.2-cm-radius racetrack is centered facing a 2.54-cm-square substrate at a separation of 8 cm. The chamber is a parallelipiped 20×20 ×8 cm. θ is the surface normal at the substrate.

$$V(r)=A\exp(-br)+(C/r)^D-(E/r)^6, \tag{7}$$

where the $(C/r)^D$ term is used to produce a smooth transition between the Born–Mayer and the r^{-6} terms. This method is, admittedly, rather ad hoc and probably inaccurate in the low-energy regime. However the results presented here were found to be insensitive to the presence or absence of the attractive well; this was to be expected because the emphasis in the present work is on the high-energy part of the distribution.

C. Sputter distribution

For the nascent distribution of sputtered particles, either the analytical Thompson distribution or fractal TRIM distribution was used. The Thompson distribution is derived assuming that ejection results from the generation of atomic collision cascades, that the energy in the cascades is shared by two-body collisions, that the mean collision free path is independent of energy, and that the existence of a surface binding energy causes refraction at the surface.[11] The distribution is proportional to

$$\frac{1-[(E_b+E)/\Lambda E_1]^{1/2}}{E^2(1+E_b/E)^3}\cos(\Theta)dE\,d\Omega, \tag{8}$$

where E_b is the binding energy of the target atoms, E_1 is the energy of the incident ion, Θ is the sputtered particle's emission angle with respect to the target normal, and ΛE_1 is the maximum recoil energy. Λ is given by $4M_iM_t/(M_i+M_t)^2$, where M_i is the incident ion mass and M_t is the mass of a target atom. It should be noted that the energy and angular parts of this distribution are separable, i.e., there is no angular dependence in the energy distribution. A more accurate method for determining the nascent sputter distribution is by the transport of ions in matter simulation, or TRIM, developed by Biersack and Haggmark.[21] This is a Monte Carlo simulation of particle transport in the solid phase, analogous to the gas phase scattering routine described above. Details may be found in Ref. 21. In order to explicitly account for the roughness that realistically occurs on the sputtered surface, the standard TRIM code has been modified using techniques from fractal geometry.[12] Comparisons of fractal TRIM with standard (planar) TRIM indicate that significant differences in sputter yield and reflection probability will occur for light ions on heavy targets at low energies and grazing incident angles.[12,22] Under the conditions of the present simulation, however, planar and fractal TRIM give essentially the same results; for definitiveness, fractal TRIM is used here. We shall see that the fractal TRIM distribution differs significantly from the Thompson distribution, particularly with regard to the angular dependence of the energy distribution. These differences have important consequences for finite geometry simulations. The target (silicon) binding energy and the fractal dimension of the surface are input parameters for the fractal TRIM simulation. A best fit to the experimental sputter yields[22] versus energy gave 5.1 eV and 2.01 for these parameters, respectively.

D. Calculation

For the present simulations, the geometry given in Fig. 2 was used. The sputtering source was a 5.08-cm-diam circular silicon target, with a magnetron "racetrack" annulus as the source of the sputtered atoms. The midpoint of the racetrack annulus was at a radius of 1.1 cm. The probability of sputtering from a given point on the racetrack was determined from a measurement of the groove depth profile on an actual sputter source. The chamber width and target-to-substrate distance were fixed at 20 and 7.5 cm, respectively; these are approximately the same dimensions of the chamber used in our film growth and mass spectrometer experiments.[15] The simulations were performed at an argon pressure of 4.5 mTorr, corresponding to a *pd* of 34 mTorr cm, and were run until 25 000 Si atoms arrived at a 6.45 cm^2 substrate centered over the sputtering target.

III. RESULTS AND DISCUSSION

A. Gas phase scattering effects

Figure 3 compares the angle-integrated energy distributions $F(E)$ [where $F(E)dE$ is the probability that a particle arrives at the substrate in the energy range between E and $E+dE$], summed over the substrate, that result from the scattering described by the three types of potentials used in this study: (a) the hard sphere, (b) the Lennard–Jones 6-12, and (c) the Abrahamson. For these three cases the fractal TRIM simulation was used for the nascent sputter distribution. For purposes of comparison, Fig. 3 also shows the energy distribution of the arrival flux when no scattering takes place.

It is observed that the unscattered flux peaks at approximately half of the Si binding energy and that it has a long high-energy tail. When scattering occurs, all distributions are shifted to lower energies. This shift is very dramatic for the hard sphere potential, while the Abrahamson potential has the smallest effect on the nascent distribution. The 6-12 potential yields a result somewhere between the

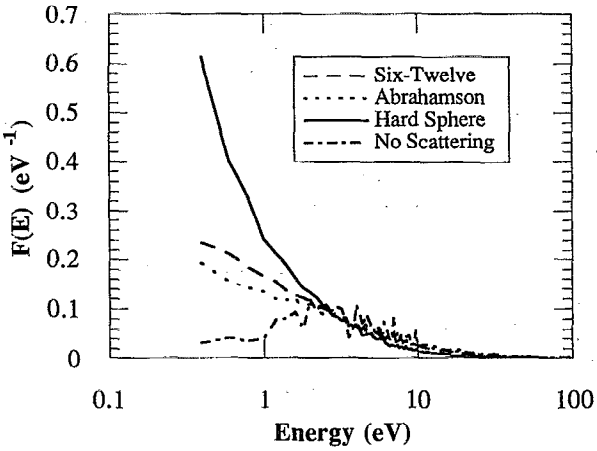

FIG. 3. Angle-integrated energy distributions of the silicon arrival flux, summed over the substrate for the hard sphere, Lennard–Jones 6-12, and Abrahamson potentials, using the geometry in Fig. 1. Fractal TRIM was used to generate the nascent sputter distribution using ions with 365 eV incident energy. Also shown is the energy distribution of the arrival flux with no gas phase scattering, corresponding to zero argon pressure.

two generated by the hard sphere and the Abrahamson potentials, but much closer to the latter. In Table I the average and global quantities determined from the energy distributions are listed.

The results in Fig. 3 and Table I indicate that the choice of gas phase interatomic potential profoundly affects the energy distribution of the arriving flux in the intermediate *pd* regime. The arrival distributions in Fig. 2 are consistent with the energy dependence of the total and differential cross sections and the energy transfer relation Eq. (4). Since the hard sphere cross section is energy independent, all sputtered atoms have equal scattering probability. In addition, the average scattering angle is large, and this results in a significant energy transfer per collision. These effects combine to produce the large downward shift in the energy distribution relative to the nascent distribution, and lower the average energy of the arrival flux. In contrast, the "softer" potentials, with their energy-dependent cross sections, allow the high-energy component of the sputtered particle distribution to move preferentially towards the substrate, while the lower-energy particles are more likely to scatter. This "energy filtering" effect is responsible for keeping the average and median energy of the arrival flux high. The scattering for the soft potentials is also more forward peaked, giving a smaller energy transfer per collision. Consequently the arrival flux is less energy degraded as compared to the hard sphere case. Inclusion of the quasithermal contribution in the energy distribution will further accentuate the differences between the potentials (last column of Table I). It is noteworthy that, although the 6-12 potential is somewhat softer than the hard sphere, there are still significant differences between the former and the more rigorous Abrahamson potential.

Another quantity of interest is the arrival probability, $p(a)$, which measures the fraction of sputtered particles that arrive onto the substrate with energies greater than 0.26 eV (Table I). The absolute value of this quantity will of course depend on the system geometry and the nascent sputter distribution, as well as the interatomic scattering potential; however, it is useful for purposes of comparison. Increasing the average scattering angle per collision by increasing the steepness of the potential will decrease $p(a)$, not only because more of the energetic flux is deflected away from the substrate, but also because more quasithermals (i.e., those sputtered atoms that have energies less than 0.26 eV) are produced as indicated in Table I. It is observed that the sputtered particles scattered by the hard sphere potential have the smallest probability of arriving at the substrate with energies above 0.26 eV, whereas those scattered by the softer potentials have arrival probabilities that are two to three times larger than those resulting from the hard sphere model.

The energy-integrated angular distribution $G(\theta)$ of the arrival flux with respect to the substrate normal is shown in Fig. 4. The unscattered flux is observed to arrive at angles less than 26.5°, corresponding to the maximum line-of-sight angle from the target racetrack. The total flux of atoms that arrive at angles less than 26.5° is made up of both directed (unscattered) and scattered components, while particles arriving at larger angles undergo at least one scattering event. It is worth noting that a purely isotropic distribution (i.e., equal arrival probability per unit solid angle) would peak at 45°, and go to zero at 0° and 90°. Such a distribution would result from a completely thermalized flux characteristic of high-pressure diode sputtering. The trends in Fig. 4 show that the steeper the potential, the faster the approach towards a more isotropic distribution, which is consistent with the discussion of the collision physics presented earlier. The smaller average cross section for the softer potential allows a larger fraction of the energetic directed flux to arrive. In addition the differential scattering cross section is more forward peaked

TABLE I. Global and average quantities for the arrival flux distribution, using the various interatomic potentials for the geometry of Fig. 1 and the conditions of Fig. 3.

Potential	Sputtered particles ($\times 10^6$)	Arrival probability	Average energy (eV)	Median energy (eV)	Average arrival angle (deg)	Percent quasithermal
No scattering	0.88	0.028	13.8	7.4	10.8	0.0
Hard sphere	4.3	0.0058	6.0	2.0	31.6	60.3
Six-twelve	1.8	0.014	11.2	4.6	27.3	28.9
Abrahamson	1.4	0.018	12.8	5.6	24.5	17.1

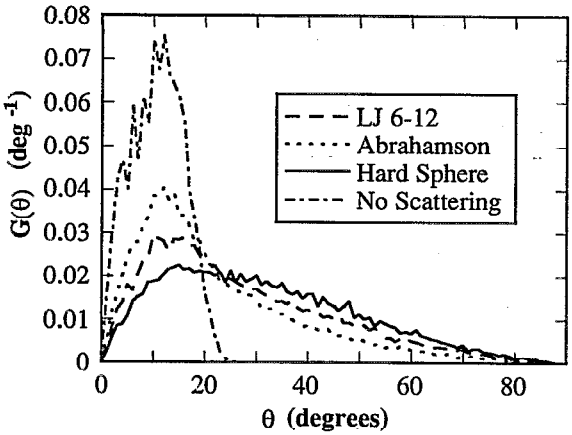

FIG. 4. Energy-integrated angular distributions of the silicon arrival flux summed over the substrate for the hard sphere, 6-12, and Abrahamson potentials, for the conditions given in Fig. 3. Also shown is the distribution for no gas phase scattering, corresponding to zero argon pressure.

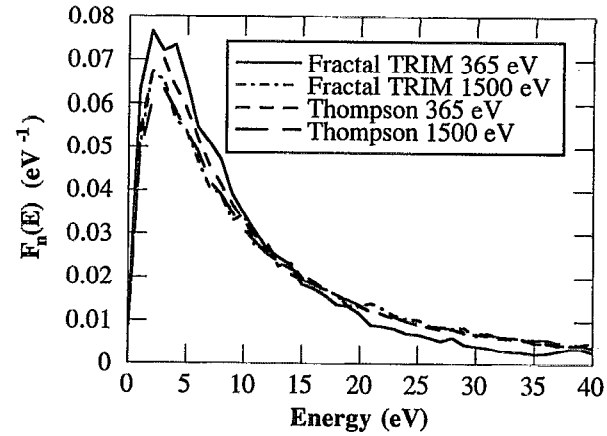

FIG. 5. Angle-integrated nascent sputtered particle energy distributions, generated by using fractal TRIM and the Thompson distribution, for incident ion energies of 365 and 1500 eV.

than that which occurs with the hard sphere. Thus, with the softer potentials, an atom is able to undergo many small angle scattering events, retain a large fraction of its energy, and still arrive with the 27° unscattered cone.

These results imply that, in this intermediate *pd* regime, use of the hard sphere potential will result in significant errors for the energy and angular distributions of the arrival flux. Although both the Lennard–Jones 6-12 and the Abrahamson TFD potentials give roughly similar results, there are still some differences between them. Of course, at much higher *pd* values, all potentials should give similar energy and angular distributions, namely an isotropic flux with a Maxwellian energy distribution (corresponding to the background gas temperature near the substrate). In this case the transport can be described by diffusion and a Monte Carlo simulation of the transport is unnecessarily computationally expensive. However, the value of *pd* that marks the transition to this regime will still depend strongly on the interaction potential used, i.e., the hard sphere potential will predict a "thermalization" *pd* that is much lower than that resulting from the softer potentials. Consequently, even in high-pressure diode sputtering, accurate potentials are required in order to determine the initial "source function" to be used in the diffusion modeling.[9,14]

B. Sputter distribution

In previously reported simulations, it has been common practice to emit the particles from the sputtering target at either a single energy, or, more realistically, by using the analytical Thompson distribution.[11] As previously mentioned, the Thompson distribution can be factored into independent energy and angular parts. A cosine angular distribution and an energy distribution independent of angle result from the assumption of isotropic recoil fluxes within the target.[23] The present TRIM simulations make no *a priori* isotropy assumptions, and should therefore provide a more accurate description of the sputtering process. If little or no difference between the fractal TRIM and Thompson distributions is observed, it may be concluded that the choice of method used to generate the nascent particle distributions is unimportant. However, any differences between the arrival fluxes would require further investigation to determine when, if ever, the use of the Thompson distribution is justified.

The nascent sputtered particle energy distributions $F_n(E)$, integrated over all ejection angles, are shown in Fig. 5 for incident ion energies of 365 and 1500 eV. This range of ion energies reflects the upper and lower bounds of typical planar magnetron deposition operating conditions. Both distributions peak at about one half the binding energy (5.1 eV) and decrease with a $1/E^2$ dependence. While the fractal TRIM distribution at 365 eV is shifted to somewhat lower energies, close agreement with the Thompson distribution is observed at 1500 eV ion energy. Similar results were obtained by Biersack and Eckstein using the TRIM.SP simulation.[24] It is worth noting that both the average and median energies of sputtered particles obtained by using each of the two distributions are also in fairly close agreement. This result demonstrates the ability of the Thompson distribution to predict angle-integrated energy distributions.

In Fig. 6 the energy-integrated probability of ejection at the angle measured with respect to the target normal, Θ, divided by the corresponding solid angle, is plotted as a function of $\cos(\Theta)$. If ejection follows a cosine distribution, then the data plotted in this manner will yield a straight line, as is the case for the Thompson distribution. The angular ejection probability obtained from using fractal TRIM is observed to deviate significantly from the cosine distribution when 365 eV ions are used for sputtering. In this case the ejection probability is under cosine at small ejection angles, while it is over cosine at large ones; the same pattern occurs with 1500 eV ions, although to a much lesser degree.

The results obtained using fractal TRIM are consistent with experimental data and other simulations reported in

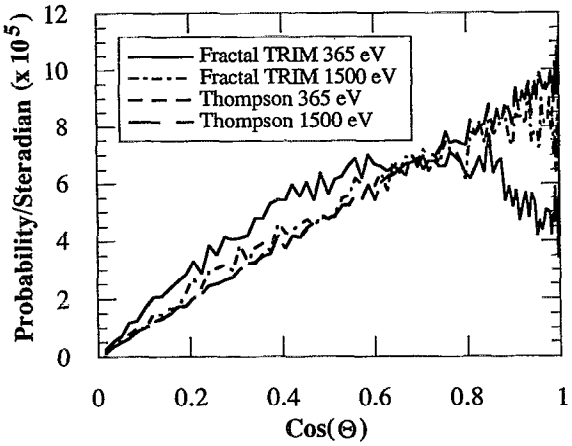

FIG. 6. Energy-integrated probability of ejection at the angle with respect to the target normal per unit solid angle vs cos(Θ), for fractal TRIM and Thompson distributions, using 365 and 1500 eV incident ions.

the literature (for a recent review see Ref. 25). For example, the experiments of Olson and co-workers[26] indicate that for low incident ion energies (< 1000 eV), the angular distribution of sputtered atoms is significantly "under cosine," Biersack and Eckstein also found under-cosine angular distributions at lower energies for Ne on Ni using the simulation TRIMSP,[24] and Robinson has obtained similar results using the MARLOWE simulation for the self-sputtering of uranium.[27] The under-cosine distribution apparently results from insufficient flux randomization during the shallow cascades.[25,27] The difference between the angular emission probabilities predicted by the simulations and the Thompson distributions could significantly affect the arrival probability of a sputtered particle onto a finite area substrate located in the chamber volume. This effect will be quantified more precisely in the next section.

In Fig. 7 the average energy at each ejection angle with respect to the target normal is plotted as a function of that angle for the same distributions shown in Fig. 6. A significant difference between the two distributions is evident.

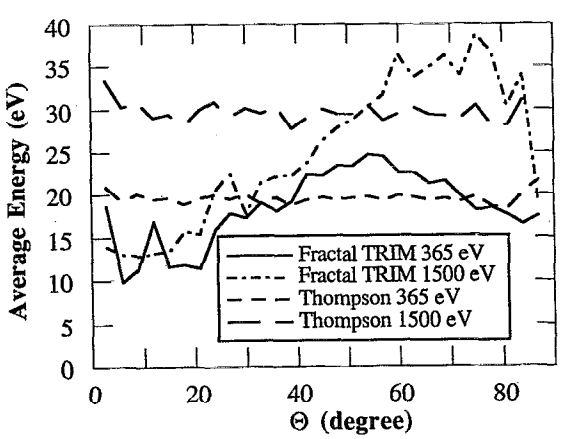

FIG. 7. Average energy vs emission angle Θ, using fractal TRIM and the Thompson distribution, for incident ion energies of 365 and 1500 eV.

TABLE II. Average and median energy as a function of the position of 1 cm^2 substrates located in a plane 7.5 cm from a 5.08-cm-diam circular magnetron. The Abrahamson potential was used for gas phase scattering with 1.5 mTorr argon, and the sputter distributions used an incident ion energy of 365 eV.

Distribution	Position from target center (cm)	Average energy (eV)	Median energy (eV)	Arrival probability
Fractal TRIM	0.0	12.2	4.2	0.026
Fractal TRIM	2.9	13.7	4.6	0.023
Fractal TRIM	5.7	18.6	5.6	0.017
Thompson	0.0	19.0	8.0	0.048
Thompson	2.9	18.2	8.0	0.038
Thompson	5.7	19.0	8.2	0.020

With increasing ejection angle, the fractal TRIM average energy is observed to initially rise, reach a maximum, and then decrease slightly. Qualitatively similar results were obtained by Eckstein using TRIMSP for 1 keV Ar on Ni.[28] As noted by Ekstein, these results imply that the energy and angular distributions are not separable, contrary to the assumption made in the analytic formulations. These results can be understood in the following way. An incoming ion's momentum will be directed 180° opposite to the direction of the target normal vector. In order for a particle to be emitted at small angles with respect to the normal, it must undergo, on average, more collisions than a particle ejected at large angles. Because the amount of energy lost by a particle will increase as the number of collisions increases, a particle ejected at large angles will, on average, be emitted at a higher energy than a particle ejected at small angles. In contrast, the Thompson formalism results in an energy distribution that is independent of angle, with the higher incoming ion energy producing an average energy that is approximately 10 eV larger.

C. System geometry

The similarities between the energy distributions shown in Fig. 5 indicate that, in simulations where infinite parallel plates are used, the Thompson and fractal TRIM distributions will give similar results, since both the angle of emission and the energy dependence on that angle are averaged out. However, with a finite system geometry, and particularly the "racetrack" geometry characteristic of magnetron sputtering, the angular dependencies observed in Sec. III B can have significant effects on the angular and energy distributions of the arrival flux. In order to test these effects, the following simulation was performed. Three separated 1 cm^2 substrates were placed, respectively, directly over, 2.9 cm away from, and 5.7 cm from the target center. All substrates were located in a plane 7.5 cm from the target. Using the Abrahamson potential to describe gas phase scattering and a low (1.5 mTorr) pressure of Ar, simulations were run using 365 eV ions for both the fractal TRIM and the Thompson distribution. The results are shown in Table II. As expected, the Thompson distribution gives results that are independent of the location of the substrate. The same is not true of the fractal TRIM

simulation; in particular, as the substrate becomes more normal to the target, a lower energy flux is intercepted, and the energy distribution gets shifted down. These results are consistent with the differences in nascent sputter distributions described in the previous section.

Thus, it may be concluded that when finite geometry is important, the Thompson distribution cannot be expected to give precise results pertaining to the energy of the depositing species at low *pd*, since the energy distribution of the arrival flux will be strongly dependent on the location of the substrate. In addition, these results imply that the energy distribution of the arrival flux on a large area substrate will not be uniform, which could lead to structural inhomogeneities in large area thin films. These effects are most pronounced when using the low-energy ions characteristic of magnetron sputtering, whereas for ion beam sputtering at several keV, these effects will be diminished.

IV. CONCLUSIONS

A comparative study of the interatomic potentials, nascent sputter distributions, and system geometry used to model low-pressure magnetron sputtering has been presented. For the intermediate *pd* regime (in this case 34 mTorr cm) the choice of interatomic potential has a large effect on the energy and angular distributions of the arrival flux. Hard sphere potentials result in large downward shifts in the energy distribution, and in considerable broadening of the angular distributions, compared to "softer" potentials such as the Lennard–Jones 6-12 and Abrahamson potentials. The softer potentials exhibit an energy filtering effect, due to the energy dependence of the collision cross section, which acts to keep the average energy high. Consequently significant errors in the energy and angular distributions, as well as the arrival probability of the depositing flux, will occur in this intermediate *pd* regime if hard sphere potentials are used.

For the nascent sputter distribution, the angle-integrated fractal TRIM distribution is in close agreement with the analytic Thompson distribution. However, the angular distribution and the angular dependence of the energy distribution were found to differ significantly between the two cases. In particular, the fractal TRIM simulation predicts both a higher probability of emission and a greater average energy at large angles with respect to the surface normal, in contrast to the Thompson distribution, which assumes an energy-independent cosine distribution. These effects, which are most pronounced at lower incident ion energies, can have a profound influence on the arrival flux for finite area substrates located at different positions in the substrate plane, as well as for different regions on a large substrate, when realistic magnetron geometries are employed.

ACKNOWLEDGMENTS

This work was supported by the Thin Film Solar Cell Program of the Electric Power Research Institute under Contract No. RP-2824-1, principal investigator J. R. Abelson. The authors are grateful for permission to use the TRIM code from the Max Planck Institut fur Plasmaphysik, Garching, Germany. Computer time was provided by the National Center for Supercomputing Applications at the University of Illinois.

[1] G. M. Turner, I. S. Falconer, B. W. James, and D. R. Mckenzie, J. Appl. Phys. **65**, 3671 (1989).
[2] T. Motohiro and Y. Taga, Thin Solid Films **112**, 161 (1984).
[3] T. Motohiro, J. Vac. Sci. Technol. A **4**, 189 (1986).
[4] M.A. Vidal and R. Asomoza, J. Appl. Phys. **67**, 477 (1990).
[5] A. M. Myers, J. R. Doyle, J. R. Abelson, and D. N. Ruzic, J. Vac. Sci. Technol. A **9**, 614 (1989).
[6] A. M. Myers, Ph.D. dissertation, University of Illinois (1991).
[7] F. J. Cadieu and N. Chencinski, IEEE Trans. Magn. **MAG-11**, 227 (1975).
[8] W. D. Westwood, J. Vac. Sci. Technol. **15**, 1 (1978).
[9] R. E. Somekh, J. Vac. Sci. Technol. A **2**, 1285 (1984).
[10] A. A. Abrahamson, Phys. Rev. **178**, 76 (1969).
[11] M. W. Thompson, Philos. Mag. **18**, 377 (1968).
[12] D. N. Ruzic, Nucl. Instrum. Methods B **47**, 118 (1990).
[13] J. F. Ziegler, J. P. Biersack, and U. Littmark, in *The Stopping and Range of Ions in Solids*, edited by J. F. Ziegler (Pergamon, New York, 1985), Vol. I , pp. 24–48.
[14] S. M. Rossnagel, IEEE Trans. Plasma Sci. **18**, 878 (1990).
[15] A. M. Myers, D. N. Ruzic, N. Maley, J. R. Doyle, and J. R. Abelson, Mater. Res. Soc. Symp. Proc. **192**, 595 (1990).
[16] J. B. Marion, *Classical Dynamics of Particles and Systems* (Academic, New York, 1970), Chap. 9.
[17] L. L. Carter and E. D. Cashwell, Particle-Transport Simulations with the Monte Carlo Method (Technical Information Center, Office of Public Affairs U.S. Energy and Research Development Administration, Oak Ridge, TN, 1975), pp. 2–11.
[18] I. Petrov (private communication).
[19] See, for example, S. Dushman, *Scientific Foundations of Vacuum Technique* (Wiley, New York, 1970), pp. 1–79.
[20] M. E. Coltrin, R. J. Kee, and J. A. Miller, J. Electrochem. Soc. **133**, 1206 (1986).
[21] J. P. Biersack and L. G. Haggmark, Nucl. Instrum. Methods **174**, 257 (1980).
[22] D. N. Ruzic, in *Handbook of Plasma Processing*, edited by S. Rossnagel, J. J. Cuomo, and W. D. Westwood (Noyes, Newark, NJ, 1990), Chap. 3.
[23] P. Sigmund, in *Sputtering by Particle Bombardment I (Topics in Applied Physics 47)*, edited by R. Behrisch (Springer, Berlin, 1981), pp. 9–71.
[24] J. P. Biersack and W. Eckstein, Appl. Phys. A **34**, 73 (1984).
[25] W. O. Hofer, in *Sputtering by Particle Bombardment III (Topics in Applied Physics 64)*, edited by R. Behrisch and K. Wittmaack (Springer, Berlin, 1991), pp. 15–90.
[26] R. R. Olson, M. E. King, and G. K. Wehner, J. Appl. Phys. **50**, 3677 (1979); G. K. Wehner, Appl. Phys. Lett. **30**, 185 (1977); G. K. Wehner and D. Rosenberg, J. Appl. Phys. **31**, 177 (1959).
[27] M. T. Robinson, J. Appl. Phys. **54**, 2650 (1983).
[28] W. Eckstein, Nucl. Instrum. Meth. Phys. Res. B **18**, 344 (1987).